2020 IEEE/RSJ International Conference on Intelligent Robots and Systems (IROS)
October 25-29, 2020, Las Vegas, NV, USA (Virtual)

Wind and the City: Utilizing UAV-Based In-Situ Measurements for Estimating Urban Wind Fields

Jay Patrikar[1], Brady G. Moon[1], and Sebastian Scherer[1]

***Abstract*— A high-quality estimate of wind fields can potentially improve the safety and performance of Unmanned Aerial Vehicles (UAVs) operating in dense urban areas. Computational Fluid Dynamics (CFD) simulations can help provide a wind field estimate, but their accuracy depends on the knowledge of the distribution of the inlet boundary conditions. This paper provides a real-time methodology using a Particle Filter (PF) that utilizes wind measurements from a UAV to solve the inverse problem of predicting the inlet conditions as the UAV traverses the flow field. A Gaussian Process Regression (GPR) approach is used as a surrogate function to maintain the real-time nature of the proposed methodology. Real-world experiments with a UAV at an urban test-site prove the efficacy of the proposed method. The flight test shows that the 95% confidence interval for the difference between the mean estimated inlet conditions and mean ground truth measurements closely bound zero, with the difference in mean angles being between -3.7° and 1.3° and the difference in mean magnitudes being between -0.2 m/s and 0.0 m/s.**

Video : https://youtu.be/U4XdYgSJRZM

I. INTRODUCTION

Enabling autonomous unmanned aerial vehicles (UAVs) to estimate wind patterns is crucial if they are to realize their potential in goods mobility, monitoring, and surveillance tasks in dense urban landscapes. Owing to their small size, low speeds, and close proximity to obstacles, the safety and operational performance of UAVs flying within cities is significantly affected by the prevailing wind conditions [1], [2]. An estimate of the wind field can provide planning and decision algorithms with necessary information to compute safer [3] and energy efficient paths [4].

UAVs are uniquely positioned to act as a source of in-situ wind measurements. This paper explores the possibility of using these local wind estimates to predict a global wind field. Wind flow estimation to enable autonomous dynamic soaring [5] has predominantly focused on estimating high altitude, clutter-free wind fields. Methods using Gaussian Process Regression [5], polynomial parameterization of the wind field [6], and Weibull probability density function with Prandtl's power law relationship [7] have been presented. Low altitude urban wind fields by comparison are more complicated and difficult to predict.

Computational Fluid Dynamics (CFD) has been presented as a promising solution to calculate the low altitude urban wind flow patterns. Techniques using Reynolds-Averaged Navier–Stokes (RANS) solvers have gained prominence over others, mainly due to their computational advantage. Using CFD results for UAV path planning has been explored in some works [1], [8], but they lack a comprehensive analysis on how close the simulation models match the real world conditions. One notable effort is made by Ware et al. [4] who validated the CFD simulation results using in-situ measurements from ground stations. The work however uses historical data for estimating the boundary conditions which may not lead to sufficiently accurate wind field predictions. Another notable effort uses high resolution wind models to provide inlet conditions to predict CNN-based wind-fields [9].

Improving the predictive accuracies of CFD simulations is

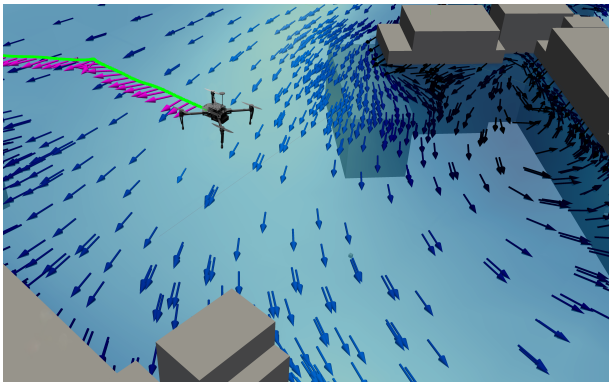

(a)

(b)

Fig. 1: (a) A CFD wind field using the estimated inlet boundary condition at the test location, along with the path of the UAV (green), and the corrected wind measurements (magenta) from the onboard anemometer. (b) The test UAV with the wind sensor.

*This work is supported by Department of Energy Grant DE-EE0008463. This material is based upon work supported by the National Science Foundation Graduate Research Fellowship under Grant No. DGE1745016.

[1]Authors are with the Robotics Institute, School of Computer Science at Carnegie Mellon University, Pittsburgh, PA, USA {jpatrika, bradym, basti}@andrew.cmu.edu

an active field of research [10]. Previous work on Uncertainty Quantification (UQ) [11] has proven that uncertainties in inlet conditions have a higher effect on the accuracy of CFD results than other parameters such as aerodynamic roughness. Other works [12] that compared CFD results with real world data have argued that even for minor changes in the inlet wind direction the simulated flow patterns can change considerably, to the extent that planning decisions might be influenced. It is thus important to have a reliable estimate of the inlet conditions. One obvious solution is to use wind sensors at the periphery of the urban area or a tall structure within the city. However, measurements from these sources can introduce considerable error as often times it is difficult to determine the errors between the incoming wind at the boundary and measured wind conditions. Jorge Sousa et al. [13] have addressed this problem of predicting the distribution of the boundary conditions (inlet speed and angle) by solving a inverse problem of estimating inlet conditions using an ensemble Kalman filter (EnKF) and given in-situ measurements from static sensors. Their subsequent work provides real world validation [14] of the methods.

This paper explores the possibility of using UAV-based sequential measurements using an onboard anemometer to solve the inverse problem of estimating the inlet boundary conditions using a particle filter (PF) based approach[1]. A PF is known to provide a better estimate of the posterior belief for low dimensional problems as it samples directly from the distribution as opposed to an EnKF which has a tendency to provide approximations to the posterior that are too close to a Gaussian distribution [17]. UAVs have an ability to fly in the roughness layer [8] that is just above the Urban Canopy Layer (UCL) and thus can potentially give a much better estimate of the inlet conditions affecting the UCL. Our setup also avoids the need of setting up a static wind measurement network, which may prove prohibitive because of cost and maintenance hurdles. As wind enters the city, it flows between structures and form a distinctive pattern. The core idea of our approach is to identify this pattern using the onboard measurements and then solve the inverse problem to estimate the inlet conditions. If the estimated boundary conditions are used as an input for running the CFD simulation, the resulting field should most closely resemble the actual wind field. The contributions of this paper are three fold:

1) We present a particle filter approach to solve the inverse problem of estimating the boundary conditions given sequential in-situ wind measurements from a UAV.
2) We present a domain specific treatment to circumvent the problem of running multiple forward simulations using Gaussian process regression to maintain the real-time onboard nature of the methodology.
3) We present real world test results that prove the efficacy of the presented methodology.

[1]The choice of anemometer is for ease of prototyping but any method that provides accurate local wind measurements from onboard sensors can be used [15], [16]

The paper is organized as follows: Section II provides details on the proposed methodology along with the mathematical formulations. Section III provides details on the field trials and the results. Section IV presents the discussions and conclusions.

II. METHODOLOGY

This section details the methodology to estimate the boundary conditions given measurements from the UAV. Care was taken that the onboard algorithms are computationally tractable for any onboard computer with modest specifications. We assume the UAV to be operating at a constant altitude and consider a 2D wind field. An extension to 3D will be covered in subsequent works. The goal is to find the distribution on the wind inlet angle Θ and wind inlet magnitude U. For the case under consideration, the local wind angle θ and the local reduced velocity $u_r = \frac{u}{U}$ are only a function of the inlet wind angle. The methodology is summarized in Figure 2.

A. Mathematical Formulations

Mathematically, the problem can be stated as: Given a set of measurements $\mathbf{z_i} = \{\theta_i, u_i\}$ for $i \in [0, N]$ from the UAV such that θ_i represents the local wind angle, and u_i represents the local wind magnitude at the i^{th} data-point, find the belief $bel(\Theta_{0:i}, U_{0:i}) = p(\Theta_{0:i}, U_{0:i} \mid \mathbf{z_{1:i}})$ for $i \in [0, N]$ where Θ_i is the wind inlet boundary angle and U_i is the wind inlet magnitude after i measurements. To solve for this belief, we will perform a domain specific derivation of a particle filter approach [18].

Using the Bayes Rule we can write:

$$\begin{aligned} bel(\Theta_{0:i}, U_{0:i}) &= p(\Theta_{0:i}, U_{0:i} \mid \mathbf{z}_{1:i}) \\ &= \eta p(\mathbf{z}_i \mid \Theta_{0:i}, U_{0:i}, \mathbf{z}_{1:i-1}) p(\Theta_{0:i}, U_{0:i} | \mathbf{z}_{1:i-1}) \end{aligned} \tag{1}$$

Using the Markov property for conditional independence:

$$\begin{aligned} bel(\Theta_{0:i}, U_{0:i}) &= \eta p(\mathbf{z}_i \mid \Theta_i, U_i) p(\Theta_{0:i}, U_{0:i} | \mathbf{z}_{1:i-1}) \\ &= \eta p(\mathbf{z}_i \mid \Theta_i, U_i) p(\Theta_{0:i-1}, U_{0:i-1} | \mathbf{z}_{1:i-1}) \\ &\quad p(\Theta_i, U_i | \Theta_{0:i-1}, U_{0:i-1}, \mathbf{z}_{1:i-1}) \\ &= \eta p(\mathbf{z}_i \mid \Theta_i, U_i) p(\Theta_{0:i-1}, U_{0:i-1} | \mathbf{z}_{1:i-1}) \\ &\quad p(\Theta_i, U_i | \Theta_{i-1}, U_{i-1}) \end{aligned} \tag{2}$$

Thus, for the m^{th} particle, the weight can be calculated as

$$w_m = \eta p(\mathbf{z}_i \mid \Theta_i, U_i) \tag{3}$$

This probability distribution can be represented as a multivariate normal distribution:

$$p(\mathbf{z}_i \mid \Theta_i, U_i) = \frac{\exp -\frac{1}{2}(\mathbf{z}_i - \bar{\mathbf{z}}_i)^T \Sigma^{-1} (\mathbf{z}_i - \bar{\mathbf{z}}_i)}{\sqrt{(2\pi)^2 \mid \Sigma \mid}} \tag{4}$$

Where

$$\bar{\mathbf{z}}_\mathbf{i} = f(\Theta_i, U_i, \mathbf{X_i}) \tag{5}$$

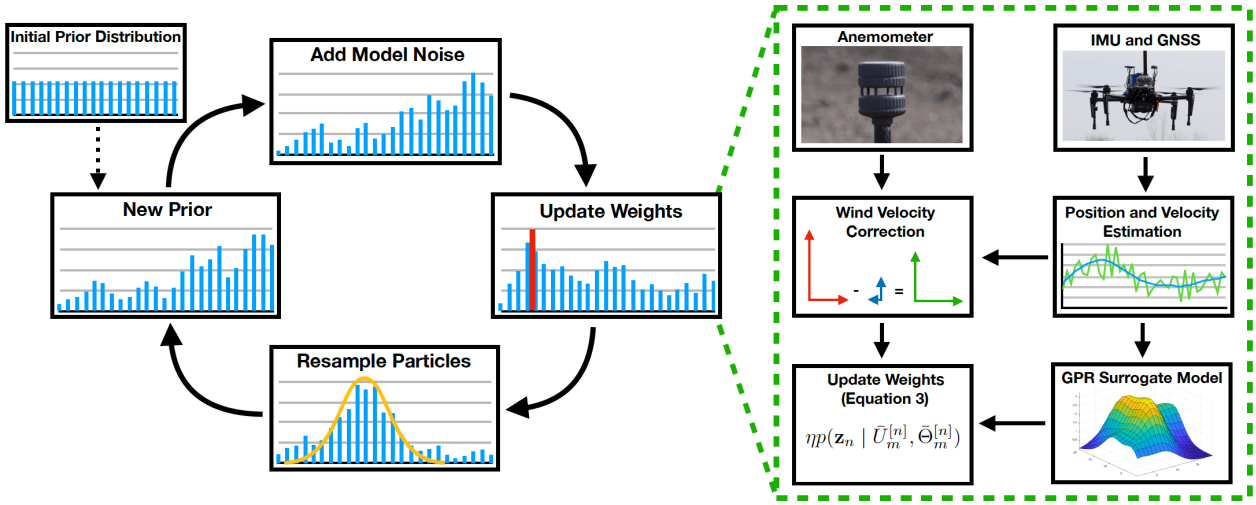

Fig. 2: Wind measurements from an onboard anemometer are corrected for motion and bias. These measurements are then used in a Particle Filter framework to provide a posterior distribution on the inlet conditions by comparing with estimates from a Gaussian Process based forward propagation model.

where $\mathbf{X_i} = \{x_i, y_i\}$ are the coordinates of the UAV when the measurement $\mathbf{z_i}$ was taken. This function is the forward model and requires running the CFD solver, but given that it is a computationally expensive operation, we instead use a computationally cheaper but less accurate surrogate function. The details are further discussed in Section II-C

B. Particle Filter

The particle filter implementation is detailed in Algorithm 1. M particles are initialized from a uniform distribution between minimum and maximum values. Each particle is a tuple of inlet angle and magnitude. The algorithm has three major components. The propagation step is the first step (Line 3), which in this case only involves adding zero mean Gaussian noise to the particles. This helps to avoid premature convergence. The next step (Line 5) involves calculating the weight of each particle based on how likely the particle represents the actual value of the inlet conditions. This weight is calculated for each particle using Equations 5 & 4. Finally based on the calculated weights, a re-sampling algorithm chooses particles for the next iteration based on the weighted probability distribution. The resampling process accounts for the difference of the target and the proposal distribution. To improve performance, we use a low-variance resampling strategy [18] to sample the distribution, as it helps preserve the diversity if samples have same importance factors and is a more systematic way for re-sampling than the independent random sampler. The sampler operates by choosing a random number between $[0, M^{-1}]$ and then repeatedly adds M^{-1} to the random number while selecting particles that correspond to the resulting summation. For the sake of brevity, the complete algorithm is not presented, and the reader is directed to Table 4.4 [18] for a detailed explanation.

Algorithm 1: Particle Filter

Input: $\mathbf{z_{1:N}}$, $[\{x_1, y_1\}, \ldots, \{x_N, y_N\}]$

1 $(U_{0:M}^{[0]}, \Theta_{0:M}^{[0]}) \leftarrow$ UniSample([0,U_{max}],[0,2π],M)

2 **for** $n \leftarrow 1$ **to** N **do**

3 $\quad(\bar{U}_{0:M}^{[n]}, \bar{\Theta}_{0:M}^{[n]}) = (U_{0:M}^{[n-1]}, \Theta_{0:M}^{[n-1]}) + \mathcal{N}(0, \sigma)$

4 $\quad$**for** $m \leftarrow 1$ **to** M **do**

5 $\quad\quad w_m = \eta p(\mathbf{z}_n \mid \bar{U}_m^{[n]}, \bar{\Theta}_m^{[n]})$

6 $\quad$**end**

7 $\quad(U_{0:M}^{[n]}, \Theta_{0:M}^{[n]}) \leftarrow$ ReSample($\bar{U}_{0:M}^{[n]}, \bar{\Theta}_{0:M}^{[n]}, w_{0:M}$)

8 **end**

C. Surrogate function

Calculating Equation 5 can prove to be a computationally expensive process, as it involves running a forward pass of the CFD simulation for the particular inlet condition and probing the location for the wind angle and magnitude. One way to avoid this issue, is to use a surrogate function to approximate these values. Jorge Sousa et al. [13] use a set of CFD simulations to construct polynomial chaos expansions (PCE) for the quantities of interest. For our use case, the PCE method gave a less accurate result, as the function variables also include the location along with the inlet angle. We decided to use a Gaussian Process Regression (GPR) to model the surrogate functions, as they have been shown to better represent spatial data. Two GPR models are trained: one for the local wind angles $\hat{f}_\theta$ and one for local wind reduced velocity $\hat{f}_{u_r}$. Both are functions of the inlet angle

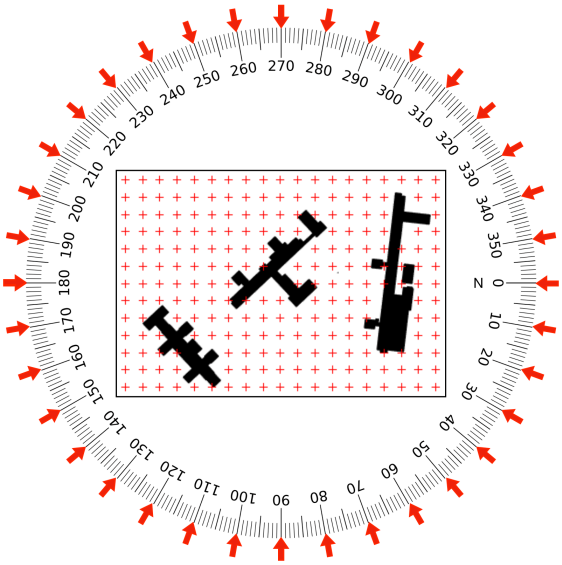

Fig. 3: Data points (locations and inlet angles) for GPR training.

and probe location. Thus Equation 5 is replaced by:

$$\begin{aligned} \bar{u}_i &= \hat{f}_{u_r}(\Theta_i, \mathbf{X}_i) U_i \\ \bar{\theta}_i &= \hat{f}_{\theta}(\Theta_i, \mathbf{X}_i) \end{aligned} \tag{6}$$

The datapoints used to train the GPR models were obtained by running multiple CFD simulations with regularly spaced inlet angles and recording data on an equally spaced grid. The data-points are visually represented in Figure 3. The performance of the GPR models is discussed in Section III-B.1.

D. Wind Measurements and Correction

Wind measurements are obtained from an ultrasonic anemometer onboard the UAV. The anemometer records the wind angle and magnitude with respect to the moving drone. Previous works that have used anemometers for onboard wind measurements [19]–[21] have reported that while the wind angle measurements were found to be accurate for all flight conditions, the magnitude measurements show a bias that reports a higher wind magnitude than expected. We found that the effect is more pronounced at lower UAV speeds. Thus, in order to record reliable wind measurements we need to remove the magnitude bias in addition to correcting for the UAV motion. The correction is given by:

$$\begin{aligned} w_N &= (w_m^{[raw]} - \alpha)\cos(w_\theta^{[raw]}) - V_N \\ w_E &= (w_m^{[raw]} - \alpha)\sin(w_\theta^{[raw]}) - V_E \\ w_m^{[corrected]} &= \sqrt{w_N^2 + w_E^2} \\ w_\theta^{[corrected]} &= \arctan(w_E, w_N) \end{aligned} \tag{7}$$

where V_N and V_E represent the inertial speed of the UAV in North and East directions, and w_N and w_E represent the corrected wind components in North and East directions. α is the bias correction factor. The value of the bias correction factor was hand tuned using historical data of similar setups [20] and nil wind observations.

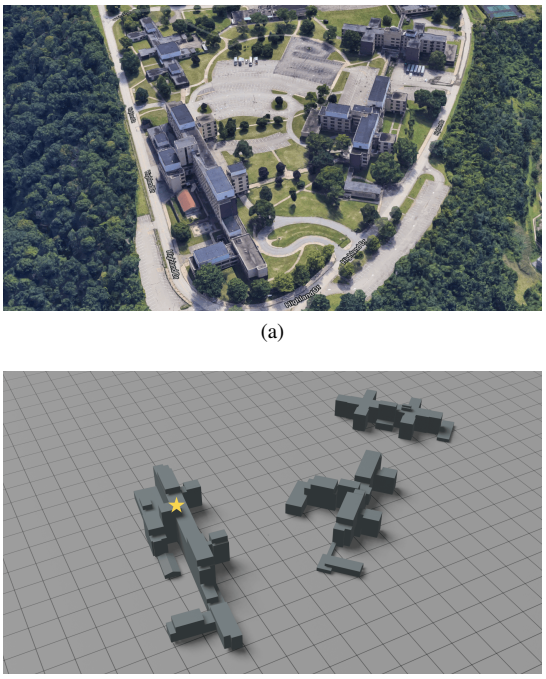

(a)

(b)

Fig. 4: (a) Image of the field validation test site. (b) 3D model of test site. Yellow star represents the location of the ground truth weather station on the top of the building.

E. Summary

The methodology assumes that an accurate 3D model of the environment is available, and the UAV has a sensor suite capable of reliably measuring the local wind angle and magnitude. The steps are as follows:

1) Given the 3D model, run multiple forward RANS CFD simulations to collect data points (Fig. 3) for training the surrogate GPR models represented in Equation 6.
2) As the UAV is flying in the flow field, collect the raw wind measurements and correct them using Equation 7.
3) Use the offline trained surrogate models and the corrected wind measurements to estimate the inlet conditions using Algorithm 1.
4) Use the inlet conditions (and the distribution) to select the correct wind-field estimate precomputed from a external high-fidelity CFD solver.

III. FIELD VALIDATION

This section gives details on the test setup and the hardware used for field validation of the algorithm. Discussion on the experiments and results follows. Field trials involve autonomously flying a predetermined sequence of waypoints and estimating the inlet conditions. For validation, the estimated inlet conditions are compared to a static wind sensor mounted on a rooftop nearby. The static wind sensor is measuring the free-stream wind magnitude and direction.

A. Setup

1) Test site: Our chosen test site is located on an elevated piece of land with around ten buildings, all ranging in heights of 5 to 35 meters (H_{max}). The buildings are abandoned and only authorised personnel are allowed within the area. The complex of buildings effectively replicates a typical urban environment and will allow for complex interactions of the wind and buildings. Because the test site is elevated from the surroundings, it provides an ideal environment to minimize disturbances to the inlet conditions.

An image and model of the test site are seen in Figure 4a and 4b respectively. The size of the site is roughly 300×250 meters. To serve as a ground truth for the inlet conditions, a weather station was placed in the location marked with a star in Figure 4b on top of the tallest building. Given the proximity of the ground weather station to the testing site and the elevated nature of land, the weather station can provide accurate measurements of inlet angles.

2) Hardware setup: Our UAV test platform is a DJI M100 quadrotor with a FT Technologies FT205EV Lightweight Ultrasonic Wind Sensor. This wind sensor is ideal for mounting on a flying platform because of its low weight and integrated magnetometer. To minimize disturbances from the quadrotor propellers, the sensor is mounted on a 40 cm long carbon fiber pole. Figure 1b shows the UAV with the sensor. The DJI SDK fuses GPS and IMU data to provide the position and velocity estimates.

For our static weather station we used a Maximet GMX500 which has a resolution of 0.01 m/s and an accuracy of $\pm 3\%$. From the station we recorded wind heading and wind magnitude, as well as the UTC time, using a single board computer. The inlet estimates from the UAV and the static measurements are synced using the GPS time on the static sensor. To reduce the high frequency noise, all the sensor measurements are passed through a median filter before using them in the algorithms.

B. Preprocessing

1) GPR Models: In order to successfully test the methodology, GPR models need to be trained to estimate the wind angles and reduced velocities given the inlet angles for the area under consideration. To generate the training data, we run CFD simulations on regularly spaced inlet angles spanning from 0° to 360° with a step size of 10°. To sample points spatially, a regularly spaced 20 m resolution grid in X and Y was used as probe locations. Figure 3 shows these points in red. Care was taken to remove points that fall within structures. CFD simulations were carried out using the OpenFoam `SIMPLE` solver [22]. The mesh was created using SnappyHexMesh. The CFD assumes in-compressible flows, and the values are recorded at steady state. A standard $\kappa - \epsilon$ model is used to model the turbulence characteristics.

The GPR models use a radial basis function (RBF) with a length scale of 10 as the kernal function. The training is carried out using the `sklearn` library [23]. To test the model performance, we plot both the angle and reduced magnitude predictions against CFD results in Figures 7 and 9 respectively.

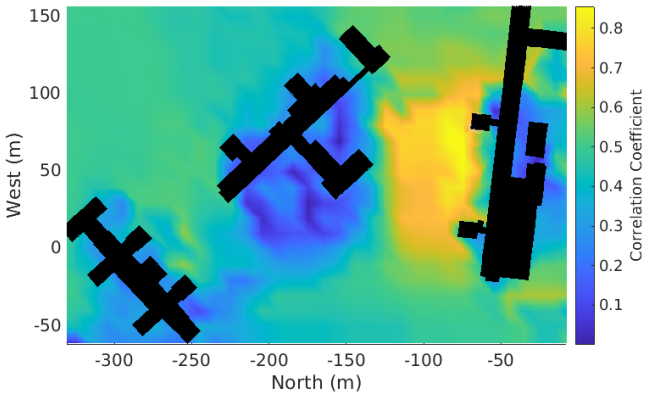

Fig. 5: Correlation between local wind angles and inlet wind angles.

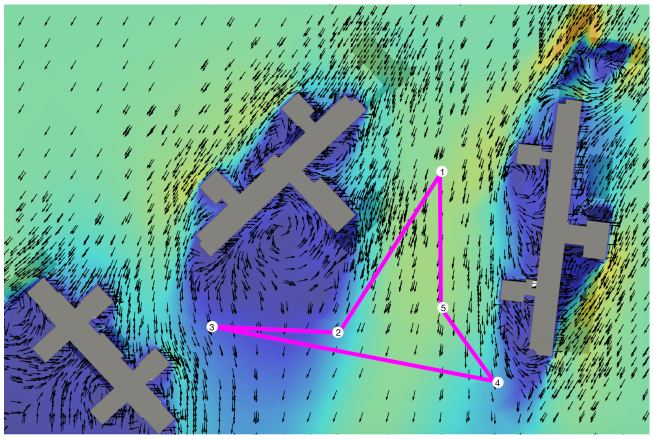

Fig. 6: The path followed autonomously by the UAV at the test site. The waypoints are numbered in the order they were visited. The arrows show the wind field flow directions, while the color gradient represent the magnitudes.

2) Correlation analysis: To identify which areas in the map are the most informative, the correlation between local wind angles and inlet angles was evaluated across the test space. For each point in a five-meter spaced grid, a Pearson correlation coefficient was calculated between the local wind angles and inlet angles. Figure 5 shows the correlation coefficients across the test space. This shows how areas which are often blocked from the wind will not correlate well to the inlet angle, and taking measurements there would not be as beneficial for inlet condition estimation. In contrast, there are also areas with high correlation, which are usually areas where the wind will be less hindered regardless of the inlet conditions. In the case of our test site, the center has the highest correlation, as well as the spaces farther out from the buildings.

C. Experiments

For the experiments, a set of waypoints for the UAV path were selected based on the correlation graph. The resulting

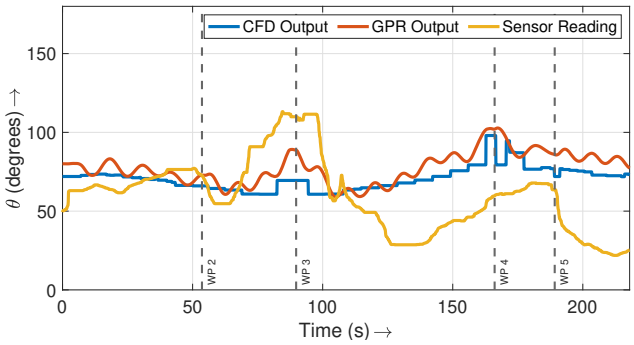

Fig. 7: The motion and bias corrected local wind angle readings for the test run. Also shown is the CFD and GPR output for the same locations as the test run using the mean of the inlet ground truth measurements.

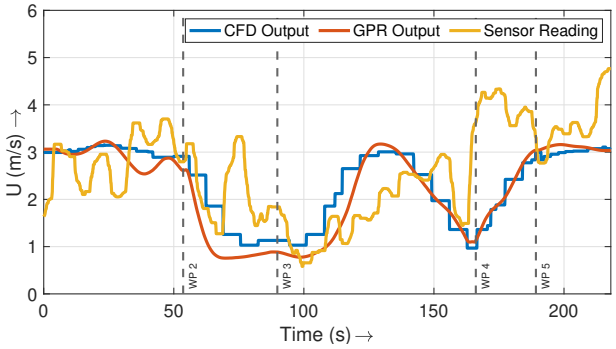

Fig. 9: The motion and bias corrected local wind magnitude readings for the test run. Also shown is the CFD and GPR output for the same locations as the test run using the mean of the inlet ground truth measurements.

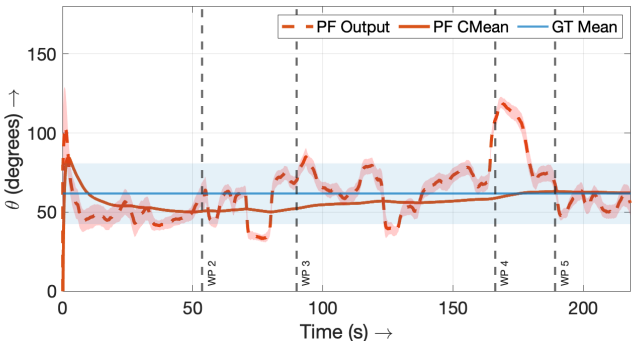

Fig. 8: The wind inlet angle (and one std. deviation) estimated from the particle filter and the mean inlet angle (and one std. deviation) measured by the ground truth weather station.

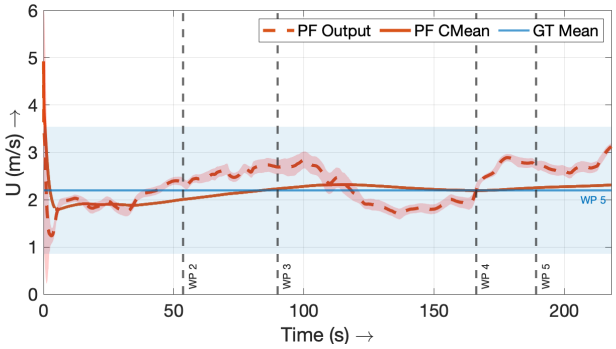

Fig. 10: The wind inlet magnitude (and one std. deviation) estimated from the particle filter and the mean inlet magnitude (and one std. deviation) measured by the ground truth weather station.

path can be seen in Figure 6. The commanded altitude of the path was 20 meters AGL, and it was flown at a commanded inertial speed of 2 m/s. The path was flown autonomously, and the corrected wind angle and speed are shown in Figures 7 and 9 respectively. The data from the the weather station was recorded concurrently for comparison. In order to match the training of the surrogate function, the wind measurements while the UAV was on the ground, taking off, and landing were not used in the particle filter, but rather only the measures when the UAV was at the commanded flight path altitude.

D. Results

The estimated inlet angle and magnitude for a test run with moderate wind speeds are plotted in Figures 8 and 10 respectively. The figures show that the estimated inlet conditions are in agreement with the values seen by the onboard anemometer. The figures also show the mean and one standard deviation of the ground truth measurements. As comparison, the cumulative means and one standard deviation of the PF output is plotted. It is clear that the mean of the PF outputs converge to the mean of the ground truth measurements. The 95% confidence interval for the difference between the mean estimated inlet angle and mean ground truth angle is $-3.680°$ and $1.250°$. The 95% confidence interval for the difference between the mean estimated inlet magnitude and mean ground truth magnitude is -0.206 m/s and 0.020 m/s. Zero lies within the bounds of both confidence intervals, thus showing the statistical significance of these results. With unoptimized code and $M = 1000$, each pass of the PF takes 277 milliseconds on an Intel NUC8i5BEK with a processor base frequency of 2.30 GHz.

IV. Conclusions and Future Work

A method to use onboard wind measurements from a UAV to solve the inverse problem of estimating the inlet conditions to improve CFD-based wind field estimation is presented. The work shows that it is possible to reliably use an anemometer on a moving UAV platform as sources of local wind measurements. The measurements are then used in a particle filter to provide a posterior distribution of the inlet conditions. A Gaussian Process Regression model is used as a surrogate function to achieve real-time performance. The method is implemented on a multirotor platform and the

results are shown to be consistent with the measurements from a static roof mounted weather station.

While the initial results are encouraging, more comprehensive testing at low and high wind conditions needs to be undertaken to fully evaluate the efficacy of the approach. The current approach considers a constant altitude 2D wind field. Extension to 3D will involve training the surrogate GPRs with an additional variable which might have a negative impact on the training accuracy. Replacing GPRs with a CNN-based surrogate model [9] might be a possible solution. Future iteration would also involve replacing the anemometer with an algorithm that uses onboard sensors (GNSS, IMU, ..) to improve accuracy and enable wider commercial adoption.

REFERENCES

[1] D. Galway, J. Etele, and G. Fusina, "Modeling of urban wind field effects on unmanned rotorcraft flight," *Journal of aircraft*, vol. 48, no. 5, pp. 1613–1620, 2011.

[2] B. Z. Cybyk, B. E. McGrath, T. M. Frey, D. G. Drewry, J. F. Keane, and G. Patnaik, "Unsteady airflows and their impact on small unmanned air systems in urban environments," *Journal of Aerospace Information Systems*, vol. 11, no. 4, pp. 178–194, 2014.

[3] M. Kothari, I. Postlethwaite, and D.-W. Gu, "Uav path following in windy urban environments," *Journal of Intelligent & Robotic Systems*, vol. 74, no. 3-4, pp. 1013–1028, 2014.

[4] J. Ware and N. Roy, "An analysis of wind field estimation and exploitation for quadrotor flight in the urban canopy layer," in *2016 IEEE International Conference on Robotics and Automation (ICRA)*. IEEE, 2016, pp. 1507–1514.

[5] N. Lawrance and S. Sukkarieh, "Simultaneous exploration and exploitation of a wind field for a small gliding uav," in *AIAA Guidance, Navigation, and Control Conference*, 2010, p. 8032.

[6] J. W. Langelaan, J. Spletzer, C. Montella, and J. Grenestedt, "Wind field estimation for autonomous dynamic soaring," in *2012 IEEE International conference on robotics and automation*. IEEE, 2012, pp. 16–22.

[7] L. Rodriguez, J. A. Cobano, and A. Ollero, "Wind field estimation and identification having shear wind and discrete gusts features with a small uas," in *2016 IEEE/RSJ International Conference on Intelligent Robots and Systems (IROS)*. IEEE, 2016, pp. 5638–5644.

[8] M. W. Orr, S. J. Rasmussen, E. D. Karni, and W. B. Blake, "Framework for developing and evaluating mav control algorithms in a realistic urban setting," in *Proceedings of the 2005, American Control Conference, 2005.* IEEE, 2005, pp. 4096–4101.

[9] F. Achermann, N. R. Lawrance, R. Ranftl, A. Dosovitskiy, J. J. Chung, and R. Siegwart, "Learning to predict the wind for safe aerial vehicle planning," in *2019 International Conference on Robotics and Automation (ICRA)*. IEEE, 2019, pp. 2311–2317.

[10] A. Ricci, I. Kalkman, B. Blocken, M. Burlando, and M. Repetto, "Impact of turbulence models and roughness height in 3d steady rans simulations of wind flow in an urban environment," *Building and Environment*, vol. 171, p. 106617, 2020.

[11] C. García-Sánchez, D. Philips, and C. Gorlé, "Quantifying inflow uncertainties for cfd simulations of the flow in downtown oklahoma city," *Building and environment*, vol. 78, pp. 118–129, 2014.

[12] D. Wise, V. Boppana, K. Li, and H. Poh, "Effects of minor changes in the mean inlet wind direction on urban flow simulations," *Sustainable cities and society*, vol. 37, pp. 492–500, 2018.

[13] J. Sousa, C. García-Sánchez, and C. Gorlé, "Improving urban flow predictions through data assimilation," *Building and Environment*, vol. 132, pp. 282–290, 2018.

[14] J. Sousa and C. Gorlé, "Computational urban flow predictions with bayesian inference: Validation with field data," *Building and Environment*, vol. 154, pp. 13–22, 2019.

[15] T. Niedzielski, C. Skjøth, M. Werner, W. Spallek, M. Witek, T. Sawiński, A. Drzeniecka-Osiadacz, M. Korzystka-Muskała, P. Muskała, P. Modzel, *et al.*, "Are estimates of wind characteristics based on measurements with pitot tubes and gnss receivers mounted on consumer-grade unmanned aerial vehicles applicable in meteorological studies?" *Environmental monitoring and assessment*, vol. 189, no. 9, p. 431, 2017.

[16] M. Marino, A. Fisher, R. Clothier, S. Watkins, S. Prudden, and C. S. Leung, "An evaluation of multi-rotor unmanned aircraft as flying wind sensors," *International Journal of Micro Air Vehicles*, vol. 7, no. 3, pp. 285–299, 2015.

[17] A. S. Stordal, H. A. Karlsen, G. Nævdal, H. J. Skaug, and B. Vallès, "Bridging the ensemble kalman filter and particle filters: the adaptive gaussian mixture filter," *Computational Geosciences*, vol. 15, no. 2, pp. 293–305, 2011.

[18] S. Thrun, W. Burgard, and D. Fox, *Probabilistic robotics*. MIT press Cambridge, 2000, vol. 1.

[19] O. Garibaldi Castillo and E. Londner, "Uav flight testing with an airborne sonic anemometer, imu and gps," in *28th AIAA Applied Aerodynamics Conference*, 2010, p. 4572.

[20] P. Bruschi, M. Piotto, F. Dell'Agnello, J. Ware, and N. Roy, "Wind speed and direction detection by means of solid-state anemometers embedded on small quadcopters," *Procedia Engineering*, vol. 168, pp. 802–805, 2016.

[21] R. L. Thorpe, M. McCrink, and J. W. Gregory, "Measurement of unsteady gusts in an urban wind field using a uav-based anemometer," in *2018 Applied Aerodynamics Conference*, 2018, p. 4218.

[22] (2020) OpenFOAM. [Online]. Available: www.openfoam.org

[23] F. Pedregosa, G. Varoquaux, A. Gramfort, V. Michel, B. Thirion, O. Grisel, M. Blondel, P. Prettenhofer, R. Weiss, V. Dubourg, J. Vanderplas, A. Passos, D. Cournapeau, M. Brucher, M. Perrot, and E. Duchesnay, "Scikit-learn: Machine learning in Python," *Journal of Machine Learning Research*, vol. 12, pp. 2825–2830, 2011.